*applied sciences*

MDPI

*Communication*

# Analysis of Wideband Scattering from Antenna Based on RFGG-FG-FFT with Cube Polynomial Inter/Extrapolation Method

**Weibin Kong *, Yongtao Zheng, Yubin Song, Zhongqing Fang, Xiaofang Yang and Haonan Zhang**

Research Center of Photoelectric and Information Technology, Yancheng Institute of Technology, School of Information Engineering, Yancheng 224051, China
* Correspondence: kongweibin@ycit.cn

**Abstract:** This paper presents an efficient real-coefficient fitting both Green's function and its gradient with Fast Fourier Transform (RFGG-FG-FFT) with cube polynomial inter/extrapolation method (CPIE), which is established for the analysis of scattering from antenna over a wide frequency. To improve the computation efficiency, the CPIE is utilized. In order to reduce memory requirements and accelerate matrix vector multiplication, the RFGG-FG-FFT is adopted. The accuracy, correctness and efficiency of the new method are researched on some examples. Compared with the direct method, the examples show that the new method is superior in broadband without loss of accuracy.

**Keywords:** impedance matrix; MoM; RFG-FFT; cube polynomial inter/extrapolation method (CPIE)

check for updates

**Citation:** Kong, W.; Zheng, Y.; Song, Y.; Fang, Z.; Yang, X.; Zhang, H. Analysis of Wideband Scattering from Antenna Based on RFGG-FG-FFT with Cube Polynomial Inter/Extrapolation Method. *Appl. Sci.* **2022**, *12*, 10298. https://doi.org/10.3390/app122010298

Academic Editor: Yan Zhang

Received: 19 September 2022
Accepted: 10 October 2022
Published: 13 October 2022

**Publisher's Note:** MDPI stays neutral with regard to jurisdictional claims in published maps and institutional affiliations.



## 1. Introduction

The method of moments (MoM) [1] are competent candidates for various electromagnetic radiation and scattering problems of the objects. In the MoM, the surface integral equation (SIE) is usually convenient to be applied. In addition, the MoM consumes a lot of memory required and CPU time, when the scale of solution is large. To date, a large number of the fast algorithms have been developed to accelerate the solving large-size electromagnetic problems [2,3], such as the fast Fourier transform (FFT) based algorithms (P-FFT, AIM, FGG-FG-FFT, IE-FFT, etc. [4–12]) and the fast multipole method based algorithms [13,14], etc.

In addition to these acceleration technologies, researchers also focus on improving the computational efficiency. Even if skeletonization [15] and adaptive cross approximation algorithm [16,17], etc. are used, broadband scattering calculation still requires a lot of time. Some interpolation techniques, such as fast kernel-independent modeling [18], asymptotic waveform evaluation (AWE) [4,19], skeleton based broadband algorithm [20], reduced basis method (RBM) [21,22], interpolation method [23], model-based parameter estimation (MBPE) [24], and Clenshaw-Lord-type Pade-Chebyshev approximation [25], etc. have been developed with a view to improve the efficiency of computation.

To quickly solve the problem of the broadband electromagnetic scattering, the RFGG-FG-FFT combined with the CPIE is proposed in this paper. In this way, the broadband electromagnetic scattering of objects can be calculated with only one grid generation. The CPIE is used to avoid the replicative calculations of near field impedance elements. The RFGG-FG-FFT not only reduces memory requirements but also speeds up matrix vector multiplications.

## 2. Method of Moments of Electromagnetic Field

According to the boundary condition, the magnetic field integral equation (MFIE) and electric field integral equation (EFIE) are established as:

$$\vec{E}^{in}(\vec{r})|_{\tan} = j\omega\mu \int_S [\vec{J}_S(\vec{r}') + \frac{1}{k^2}\nabla(\nabla'\vec{J}_S)]G(\vec{r},\vec{r}')d\vec{r}'|_{\tan} \quad (1)$$

$$\hat{n} \times \vec{H}^{in} = \frac{\vec{J}_S(\vec{r}')}{2} - \hat{n} \times P.V.\int_S \vec{J}_S(\vec{r}') \times \nabla G(\vec{r},\vec{r}')d\vec{r}' \quad (2)$$

where $P.V.$ is Cauchy Principal value integral in Equation (2) $k$ and $\eta$ are wave number and wave impedance, $G(\vec{r},\vec{r}')$ is Green's function in the free space. $\vec{J}_S$ represent current densities on surface.

In order to solve Equations (1) and (2), triangular patches are used to discrete the surface. The RWG basis functions [1] are defined on triangular patches. Hence the current vector $I$ can be expressed into

$$I \approx \sum_{n=1}^{N} I_n \vec{J}_n\left(\vec{r}\right) \quad (3)$$

where $\vec{J}_n\left(\vec{r}\right)$ and $N$ are the basis function and the number of unknowns, respectively. $I_n$ is current coefficient vector. The following conclusions can be drawn from the Galerkin test:

$$\begin{gathered} \sum_{n=1}^{N} Z_{1n} I_n = V_1, \\ \cdots \\ \sum_{n=1}^{N} Z_{Nn} I_n = V_N, \end{gathered} \quad (4)$$

where $Z_{mn}, (m = 1, 2, \cdots, N)$ means impedance matrix. $V_m$ is excitation vector. The specific form of $Z_{mn}$ is as follows

$$Z_{mn}^{EFIE} = jk\eta \int_{S_m} ds \vec{J}_m\left(\vec{r}\right) \cdot \int_{S_n} G\left(\vec{r},\vec{r}'\right)\vec{J}_n\left(\vec{r}'\right)ds' - j\frac{\eta}{k}\int_{S_m} ds\left[\nabla \cdot \vec{J}_m\left(\vec{r}\right)\right] \cdot \int_{S_n} G\left(\vec{r},\vec{r}'\right)\left[\nabla \cdot \vec{J}_n\left(\vec{r}'\right)\right]ds' \quad (5)$$

$$Z_{mn}^{MFIE} = \frac{1}{2}\int_{S_m} \vec{J}_m\left(\vec{r}\right) \cdot \vec{J}_n\left(\vec{r}\right)ds + \int_{S_m} ds\left[\hat{n} \times \vec{J}_m\left(\vec{r}\right)\right] \cdot \int_{S_n} \nabla G\left(\vec{r},\vec{r}'\right) \times \vec{J}_n\left(\vec{r}'\right)ds' \quad (6)$$

where, $\vec{J}_m\left(\vec{r}\right)$ indicate the testing functions. $S_m$ and $S_n$ are their support sets.

## 3. Interpolation Technique of MoM Matrix

According to the previous statement, Equation (4) are actually functions of frequency point $f$:

$$\sum_{n=1}^{N} Z_{mn}(f)I_n(f) = V_m(f), m = 1, 2, \cdots, N \quad (7)$$

If the wideband response is of interest, it will take more time to solve EFIE and MFIE at each $f$ using the MoM. $[f_l, f_h]$ is the frequency variation range. The object is discretized at the highest frequency $f_h$ using triangular meshes. $\lambda_h$ is the wavelength. $Z_{mn}(f)$ of EFIE and MFIE are:

$$Z_{mn}^{E}(f_r) = \int_{S_m(\lambda_h)} ds \int_{S_n(\lambda_h)} ds' \left[\vec{J}_m(\vec{r}) \cdot \vec{J}_n(\vec{r}')k_r - \nabla_h \cdot \vec{J}_m(\vec{r})\nabla'_h \cdot \vec{J}_n(\vec{r}')\frac{1}{k_r}\right]\frac{e^{-jk_r R}}{R}\frac{j\eta\lambda_h^2}{4\pi} \quad (8)$$

$$Z_{mn}^{M}(f_r) = \left[ \int_{S_m(\lambda_h)} ds \vec{J}_m(\vec{r}) \cdot \vec{J}_n(\vec{r}) - \frac{1}{2\pi} \int_{S_m(\lambda_h)} ds \vec{J}_m(\vec{r}) \cdot \hat{n} \times \int_{S_n(\lambda_h)} ds' \nabla_h \frac{e^{-jk_r R}}{R} \times \vec{J}_n(\vec{r}') \right] \frac{\eta \lambda_h^2}{2} \tag{9}$$

where $k_r = 2\pi f_r$, $f_r = f/f_h$. Therefore, the range of $f_r$ is $[f_l,/f_h, 1]$. The following changes:

$$z_{mn}^{K}(f_r) := \frac{Z_{mn}^{K}(f_r)}{\lambda_h^2} \tag{10}$$

where, the superscript $K$ represents $E, M, C$.

The phase term $e^{-jk_r R}$ can cause the fluctuation. The matrix elements are corrected by:

$$\tilde{z}_{mn}^{K}(f_r) = \begin{cases} z_{mn}^{K}(f_r) f_r e^{jk_r R_{mn}} & S_m \cap S_n = 0 \\ z_{mn}^{K}(f_r) f_r & S_m \cap S_n \neq 0 \end{cases} \tag{11}$$

$S_m$ and $S_n$ are triangles, and the relationship between them can be found in [23]. Thereby, $\tilde{z}_{mn}^{K}(f_r)$ becomes a quadratic polynomial.

The cubic polynomial interpolation/extrapolation method is mainly adopted to generate the corrected matrix at $y_v = f_v/f_h (f_v \in [f_l, f_h]; v = 0,1,2,3)$, where $f_v$ are the optimal points. The specific formula for each $f_r$ is as follows [23]:

$$\tilde{z}_{mn}^{S}(f_r) = \sum_{v=0}^{3} \tilde{z}_{mn}^{S}(y_v) \phi_v(f_r) \tag{12}$$

where,

$$\phi_k(t) = \prod_{l=0, l\neq k}^{l=3} \left( \frac{t - t_l}{t_k - t_l} \right) \tag{13}$$

## 4. RFGG-FG-FFT Algorithm

The impedance matrix $Z^C$ consists of the near field interactions $Z^{C-near}$ and the far-field interactions $Z^{C-far}$ [6,10]. In general, $\gamma \in [0,1]$ is selected as 0.5. In this way, CFIE can avoid internal resonance, thus ensuring high accuracy and small matrix condition number.

$$\begin{aligned} Z^C &\approx (Z_{MoM}^{C-near} - Z_{FFT}^{C-far}) + Z_{FFT}^{C-far} \\ &= [\gamma(Z_{MoM}^{E-near} - Z_{FFT}^{E-far}) + (1-\gamma)(Z_{MoM}^{M-near} - Z_{FFT}^{M-far})] + \gamma Z_{FFT}^{E-far} + (1-\gamma) Z_{FFT}^{M-far} \end{aligned} \tag{14}$$

In Equation (14) $Z_{MoM}^{C-near}$ is near field interaction part computed by MoM, $Z_{FFT}^{C-far}$ is the approximation by FFT-based algorithm in near field. $Z_{MoM}^{C-near} - Z_{FFT}^{C-far}$ is precorrected matrix. $Z_{MoM}^{C-near}$ and $Z_{FFT}^{C-far}$ are stored as sparse matrices. $Z_{FFT}^{E-far}$ and $Z_{FFT}^{M-far}$ are the calculated by FFT-based algorithm expressed as:

$$Z_{FFT}^{E-far} = jk\eta_0 \prod \cdot G \cdot \prod^T - j\frac{\eta_0}{k} \prod_d \cdot G \cdot \prod_d^T \tag{15}$$

$$Z_{FFT}^{M-far} = \prod_g \cdot G \prod^T \tag{16}$$

where $\prod$, $\prod_d$ and $\prod_g$ are sparse coefficient transformation matrices. $G$ are triple Toeplitz matrices (called numerical Green functions) formed by Green functions between spatial grid points. Superscript $T$ represents the transpose of a matrix. In this way, FFT can accelerate the matrix vector products of each iteration.

Let $M$ be expansion order, $C_m$ be fitting cube. $C_m$ consists of $(M+1)^3$ grid nodes. The center of $C_m$ is $c_m$. $h_x, h_y, h_z$ are Cartesian grid spacing in three coordinate directions. $\tilde{S}_m$ is testing spherical surface, which's center is $c_m$ and radius is $R_m = r_m + 0.05\lambda$. $r_m$

is the minimum radius of sphere surrounding $C_m$. $\{\vec{p}\}$ are testing points located on $\tilde{S}_m$. Therefore, $G(\vec{r}, \vec{r}')$ and $\nabla G(\vec{r}, \vec{r}')$ can be expressed as:

$$\begin{bmatrix} RG(\vec{p}, \overleftarrow{q}) \\ IG(\vec{p}, \overleftarrow{q}) \end{bmatrix} = \sum_{\vec{v} \in C_m} \pi^{\overleftarrow{q}}_{\vec{v}, C_m} \begin{bmatrix} RG(\vec{p}, \vec{v}) \\ IG(\vec{p}, \vec{v}) \end{bmatrix} \tag{17}$$

$$\begin{bmatrix} \nabla RG(\vec{p}, \overleftarrow{q}) \\ \nabla IG(\vec{p}, \overleftarrow{q}) \end{bmatrix} = \sum_{\vec{v} \in C_m} \vec{\varsigma}^{\overleftarrow{q}}_{\vec{v}, C_m} \begin{bmatrix} RG(\vec{p}, \vec{v}) \\ IG(\vec{p}, \vec{v}) \end{bmatrix} \tag{18}$$

where, $\{\pi^{\vec{r}}_{\vec{v}, C_m}\}_{u=1}^{N_c}$ and $\{\vec{\varsigma}^{\vec{r}}_{\vec{v}, C_m}\}_{u=1}^{N_c}$ are fitting coefficients. The real and imaginary part of $G(\circ)$ are $RG(\circ)$ and $IG(\circ)$.

## 5. Numerical Results

The applicability and correctness of the RFGG-FG-FFT with cube polynomial inter/extrapolation method will be tested by analyzing the scattering problems in this section. All the computation is carried out on $M = 2$ and $h_x = h_y = h_z = h$, where $M$ denotes the expansion order and $h$ denotes the Cartesian grid spacing.

### *5.1. A PEC Cube with Four Monopole Antennas*

The wideband EM scattering from 15 GHz to 30 GHz of a PEC cube ($4\lambda_h \times 4\lambda_h \times 4\lambda_h$) with four monopole antennas shown in Figure 1 is analyzed. $\Delta f = 1$ GHz is selected as the frequency interval. The cube with four monopole antennas is discretized with 23,044 triangular patches resulting into 34,566 RWG basis functions.

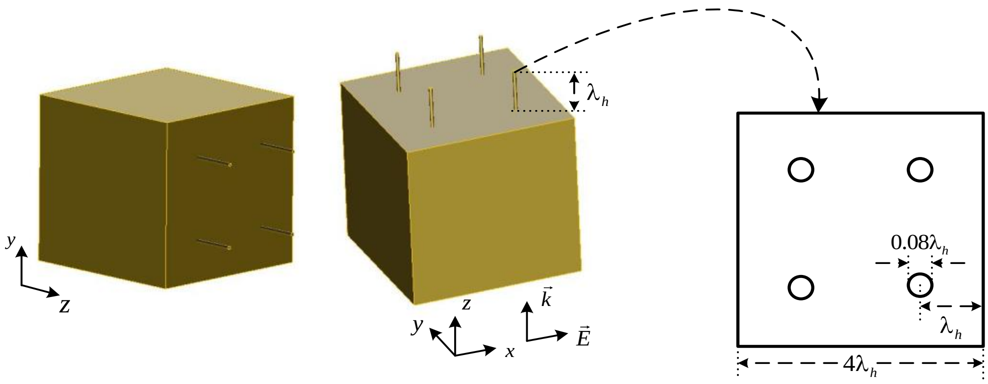


**Figure 1.** A PEC Cube with four monopole antennas.

Figures 2 and 3 show the bistatic RCS of the PEC cube with four monopole antennas obtained by direct RFGG−FG−FFT, the proposed method, FGG−FG−FFT. It can be also noted that direct RFGG-FG-FFT, the proposed method and FGG-FG-FFT gave identical numerical results. Hence, it indicates that the results of the proposed method, the direct RFGG-FG-FFT and FGG-FG-FFT are almost indistinguishable. In Table 1, the time costs of near field calculation at 24 GHz are given by direct RFGG-FG-FFT and the proposed method. The proposed method took 1307 s CPU time to obtain the results of the cube with four monopole antennas in the frequency domain, whereas the direct RFGG-FG-FFT took 2723 s. This comparison clearly shows that the proposed method can obtain the RCS simultaneous versus frequency more quickly.

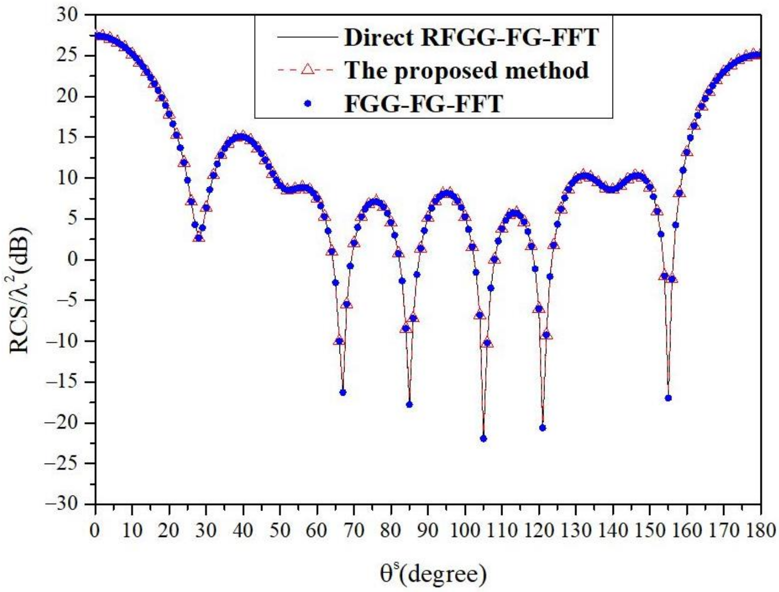


**Figure 2.** Comparisons of the bistatic RCS of PEC Cube with four monopole antennas at 17 GHz.

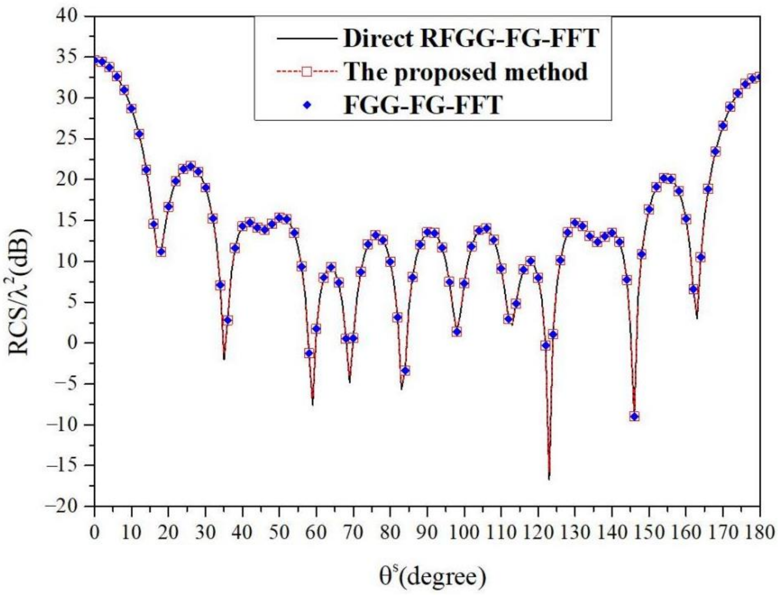


**Figure 3.** Comparisons of the bistatic RCS of PEC Cube with four monopole antennas at 26 GHz.

**Table 1.** CPU time required for the example at 24 GHz.

| Ex. | Computing Method | CPU Time Cost of $Z^{near}$(s) | CPU Time Cost of the Near Part in $Z^{far}$(s) |
|---|---|---|---|
| A PEC Cube with four monopole antennas | Direct RFGG-FG-FFT | 103 | 0.5 |
| | The proposed method | 5 | 0.5 |
| | FGG-FG-FFT | 123 | 0.7 |
| A complex combination object of monopole antenna arrays and cuboid | Direct RFGG-FG-FFT | 2320 | 46 |
| | The proposed method | 84 | 44 |
| | FGG-FG-FFT | 2718 | 63 |

### 5.2. *A Complex Combination Object of Monopole Antenna Arrays and Cuboid*

As shown in Figure 4, a complex combination object of monopole antenna arrays and cuboid is considered. The object is discretized with 30,988 triangular patches to generate

$N$ =46,482 RWG basis functions. The wideband EM scattering over 15 GHz to 30 GHz is analyzed. $\Delta f = 1$ GHz is used as the interval.

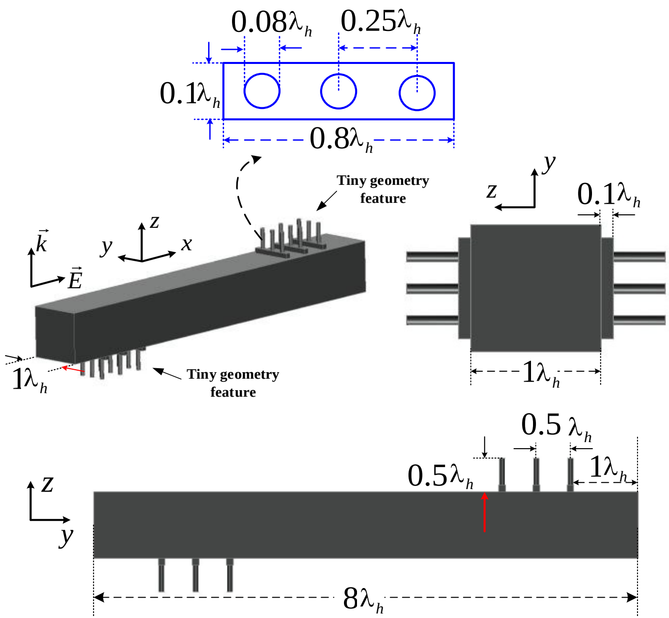


**Figure 4.** A complex combination object of monopole antenna arrays and cuboid.

The results are compared with the bistatic RCS at 19 GHz and 28 GHz is shown in Figures 5 and 6. Figure 7 shows the broadband RCS curve with scattering angle $(\theta^s, \phi^s) = (130^o, 0^o)$ obtained by using the RFGG-FG-FFT with cube polynomial inter/extrapolat- ion method, direct RFGG-FG-FFT and FGG-FG-FFT. The results obtained by three algorithms shows that they have fine consistency. It is obvious that the three sets of results agree well. Table 1 lists the CPU time costs by three methods at 24 GHz. Therefore, it can be found that the proposed method significantly enhances the computing efficiency. The CPU time required for direct RFGG-FG-FFT and the proposed method are 961 and 510 min, respectively.

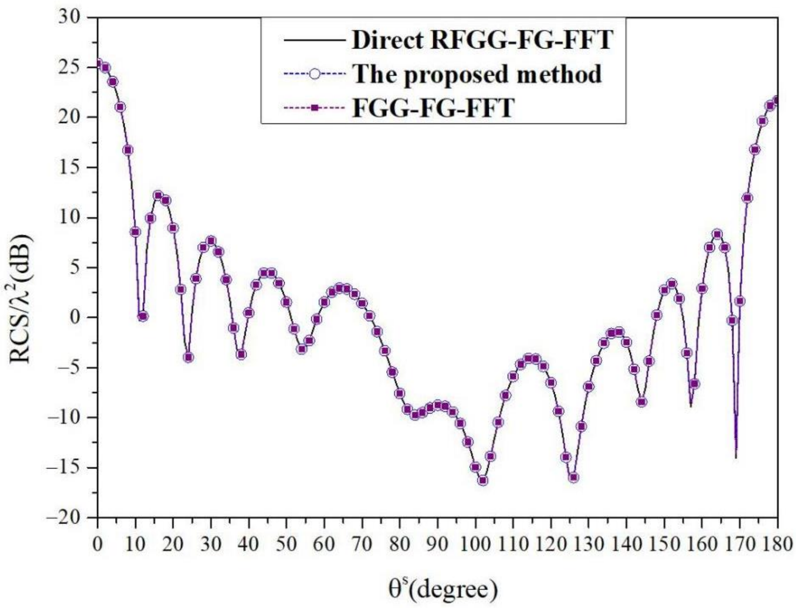


**Figure 5.** The bistatic RCS of complex combination object at 19 GHz.

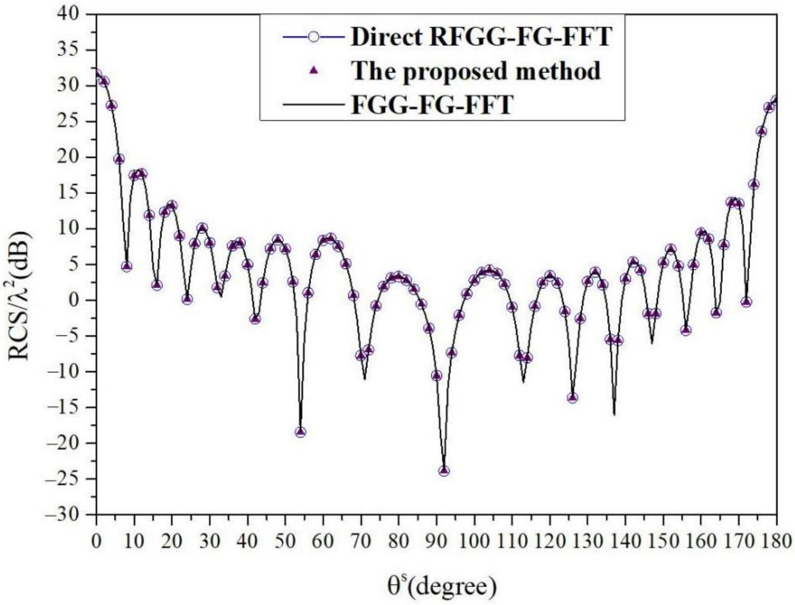


**Figure 6.** The bistatic RCS of complex combination object at 28 GHz.

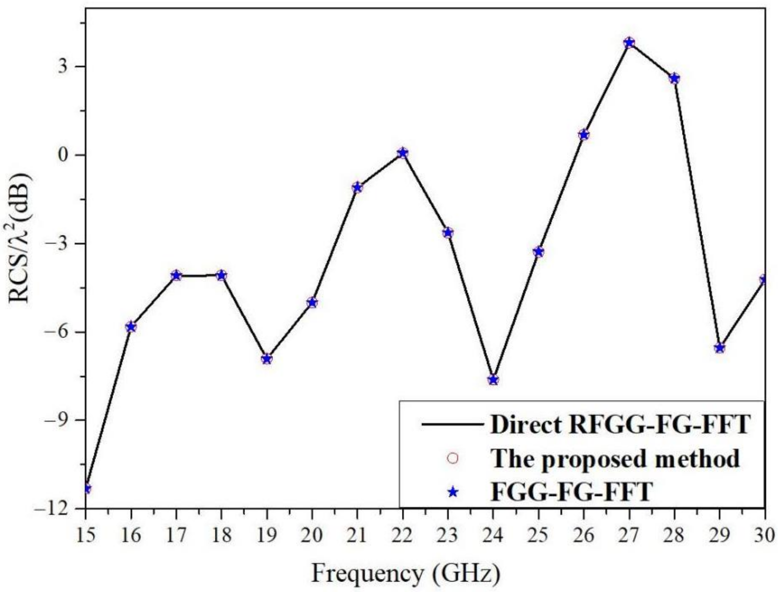


**Figure 7.** Wide frequency band RCS of complex combination object.

## 6. Conclusions

This paper proposes an effective method combining RFGG-FG-FFT with cube polynomial inter/extrapolation method for the broadband scattering of antennas. The cube polynomial inter/extrapolation method is introduced into RFGG-FG-FFT to reduce the generation time of near-field matrix. Thus, the calculation efficiency of each frequency point calculated by RFGG-FG-FFT is improved. Specifically, the calculations of the proposed scheme are very consistent with those of direct RFGG-FG-FFT and FGG-FG-FFFT. It is worth pointing out that it is a meaningful future research to solve wideband and wide-angle scattering problems rapidly by adopting integral equations.

**Author Contributions:** Conceptualization, W.K. and Z.F.; methodology, W.K. and X.Y.; algorithm implementation, W.K., Y.Z. and Y.S.; validation, Y.Z. and Y.S.; formal analysis, Y.S.; investigation, Y.Z. and H.Z.; data curation, H.Z.; writing—original draft preparation, Y.Z.; writing—review and editing, W.K.; visualization, H.Z.; supervision, X.Y.; project administration, W.K. and X.Y.; funding acquisition, W.K., Y.S. and X.Y. All authors have read and agreed to the published version of the manuscript.

**Funding:** This research was funded by the Natural Science Foundation of the Jiangsu Higher Education Institutions of China (Grant No. 19KJA110002 and 19KJB510061), the Graduate Innovation Project (SJCX22-XZ033), the Natural Science Foundation of Jiangsu Province (Grant No. BK20181050).

**Institutional Review Board Statement:** Not applicable.

**Informed Consent Statement:** Not applicable.

**Conflicts of Interest:** The authors declare no conflict of interest.

## References

1. Harrington, R.F. *Field Computation by Moment Methods*, 2nd ed.; IEEE Press: New York, NY, USA, 1993.
2. Zhang, K.; He, M.; Xu, X.W.; Sun, H.J. An efficient solution of the volume-surface integral equation for electromagnetic scattering and radiation of the composite dielectric-conductor objects with reduced number of unknowns. *IEEE Trans. Antennas Propag.* **2013**, *61*, 798–808. [CrossRef]
3. Lei, W.; Shao, H.R.; Hu, J. An efficient integral equation model-order reduction method for complex radiation problem. *IEEE Antennas Wireless Propag. Lett.* **2021**, *20*, 1205–1209. [CrossRef]
4. Dong, H.; Gong, S.; Wang, X.; Zhang, P.; Zhao, B. Efficient analysis of surface-wire configurations using AIM and best uniform rational approximation. *Chin. J. Electron.* **2015**, *4*, 215–221. [CrossRef]
5. Dong, H.; Gong, S.; Xue, H.; Wang, X.; Zhao, B.; Zhang, P. A hybrid broadband analysis approach for surface-wire junctions structures by applying AIM and asymptotic waveform evaluation technique. *J. Electromagnet. Wave.* **2016**, *30*, 141–153. [CrossRef]
6. Li, W.W.; Chen, W.; Fu, Z.J. Precorrected-FFT accelerated singular boundary method for large-scale three-dimensional potential problems. *Commun. Comput. Phys.* **2017**, *22*, 460–472. [CrossRef]
7. Wang, C.F.; Ling, F.; Jin, J.M. A fast full-wave analysis of scattering and radiation from large finite arrays of microstrip antennas. *IEEE Trans. Antennas Propag.* **1998**, *46*, 1467–1474. [CrossRef]
8. Ridene, S. Novel T-shaped GaSb/InAsN quantum wire for mid-infrared laser applications. *Phys. Lett. A* **2017**, *381*, 3324–3331. [CrossRef]
9. Rui, P.L.; Chen, R.S.; Fan, Z.H.; Yung, E.K.N.; Chan, E.C.H.; Nie, Z.P.; Hu, J. Fast analysis of electromagnetic scattering of 3-D dielectric bodies with augmented GMRES-FFT method. *IEEE Trans. Antennas Propag.* **2005**, *53*, 3848–3853. [CrossRef]
10. Sun, H.L.; Tong, C.M. Analysis of scattering from composite conductor and dielectric objects using single integral equation method and FG-FFT. *J. Electromagn. Waves Appl.* **2017**, *31*, 225–240. [CrossRef]
11. Tian, G.L.; Tong, C.M.; Peng, P.; Xie, S.J. Fast RFGG-FG-FFT/IKA for scattering from multiple targets above a rough surface. *IEEE Antennas Wirel. Propag. Lett.* **2021**, *20*, 1239–1243. [CrossRef]
12. Ridene, S. Mid-infrared emission in $In_xGa_{1-x}As/GaAs$ T-shaped quantum wire lasers and its indium composition dependence. *Infrared Phys. Technol.* **2018**, *89*, 218–222. [CrossRef]
13. Darve, E. The fast multipole method: Numerical implementation. *J. Comput. Phys.* **2000**, *160*, 195–240. [CrossRef]
14. Song, J.-M.; Lu, C.-C.; Chew, W.C. Multilevel fast multipole algorithm for electromagnetic scattering by large complex objects. *IEEE Trans. Antennas Propag.* **1997**, *45*, 1488–1493. [CrossRef]
15. Liu, Y.N.; Pan, X.M. Solution of volume-surface integral equation accelerated by MLFMA and skeletonization. *IEEE Trans. Antennas Propag.* **2022**, *70*, 6078–6083. [CrossRef]
16. Bao, Y.; Song, J.M. Multilevel kernel degeneration–adaptive cross approximation method to model eddy current NDE problems. *J. Nondestr. Eval.* **2022**, *41*, 17. [CrossRef]
17. Su, T.; Ding, D.; Fan, Z.; Chen, R. Efficient analysis of EM scattering from bodies of revolution via the ACA. *IEEE Trans. Antennas Propag.* **2014**, *62*, 983–985. [CrossRef]
18. Li, M.; Francavilla, M.A.; Chen, R.S.; Vecchi, G. Wideband fast kernel-independent modeling of large multiscale structures via nested equivalent source approximation. *IEEE Trans. Antennas Propag.* **2015**, *63*, 2122–2134. [CrossRef]
19. Wu, B.; Sheng, X. Application of asymptotic waveform evaluation to hybrid FE-BI-MLFMA for fast RCS computation over a frequency band. *IEEE Trans. Antennas Propag.* **2013**, *61*, 2597–2604. [CrossRef]
20. Pan, X.; Sheng, X. Efficient wide-band evaluation of electromagnetic wave scattering from complex targets. *IEEE Trans. Antennas Propag.* **2014**, *62*, 4304–4313. [CrossRef]
21. Fares, M.; Hesthaven, J.S.; Maday, Y.; Stamm, B. The reduced basis method for the electric field integral equation. *J. Comput. Phys. Lett.* **2017**, *16*, 825–828. [CrossRef]
22. Wu, L.F.; Zhao, Y.W.; Cai, Q.M.; Zhang, R.R.; Gu, L.; Zhang, Z.P.; Nie, Z.P. MLACE-MLFMA combined with reduced basis method for efficient wideband electromagnetic scattering from metallic targets. *IEEE Trans. Antennas Propag.* **2019**, *67*, 4738–4747. [CrossRef]

23. Li, W.D.; Zhou, H.X.; Hu, J.; Song, Z.; Hong, W. Accuracy improvement of cubic polynomial inter/extrapolation of MoM matrices by optimizing frequency samples. *IEEE Antennas Wireless Propag. Lett.* **2011**, *10*, 888–891.
24. Miller, E.K. Adaptive sparse sampling to estimate radiation and scattering patterns to a specified uncertainty with model-based parameter estimation: Compute patterns using as few as two to four samples per lobe. *IEEE Antennas Propag. Mag.* **2015**, *57*, 103–113. [CrossRef]
25. Jeong, Y.R.; Hong, I.P.; Chun, H.J.; Park, Y.B.; Kim, Y.J.; Yook, J.G. Fast scattering analysis over a wide frequency band using Clenshaw-Lord-type Pade-Chebyshev approximation. *IET Microw. Antennas Propag.* **2016**, *10*, 245–250. [CrossRef]